

Toward tunable thin-film filters for wavelength division multiplexing applications

Michel Lequime, Remy Parmentier, Fabien Lemarchand, and Claude Amra

We provide a detailed analysis of the various problems connected with the development of tunable thin-film filters for wavelength-division multiplexing applications. We examine the relation between the change in layer thickness and the central wavelength shift for various configurations and point out the significance of the structure of the reflectors, the spacer thickness, and the location of the active layers. We describe and compare practical arrangements using either temperature or an electric field as the driving parameter. © 2002 Optical Society of America

OCIS codes: 160.4670, 310.3840, 230.4170, 310.6870.

1. Introduction

Since the early 1990s, the use of wavelength division multiplexing (WDM) has allowed for a dramatic increase in the capacity of telecommunication fiber-optic networks. The practical implementation of such a technique implies the availability of a new family of devices used to combine and/or separate the various wavelength channels. These devices include multiplexers, add/drop multiplexers, and demultiplexers. Various technologies such as thin-film filters, fiber Bragg gratings, diffraction gratings, or arrayed waveguide gratings compete to achieve the manufacture of these basic components, and the choice of a technology to fulfill a given function is often the result of a compromise between performance and cost.

Moreover, the efficient exploitation of a complex fiber-optic network architecture still requires a rapid, controllable, and flexible channel routing. But all the wavelength-selective components listed above are at the present time essentially passive, and this channel routing can be achieved only if we combine them with optical switching devices using either fiber switching or wavelength conversion. The active de-

vices that result from this association are called optical cross connects (OXC).

Here we aim to provide a detailed analysis of the various concepts that allow us to fulfill the main requirements of an OXC device by using only optical interference coating technology. The key to such an approach is obviously the development of a tunable thin-film filter (TTFF) whose central wavelength can be changed by a control signal.

It is well known that a small change in the angular position of a narrow-band filter with respect to the direction of the incident light beam induces a slight shift of its central wavelength without critical degradation of other optical performances such as insertion loss, channel isolation, backreflection, and polarization-dependent losses). This property has been widely used by various manufacturers¹ for the development of tunable bandpass filters. However, this kind of solution is not compatible with the miniaturization constraints applicable to operational OXC devices and does not provide effective system improvement with regard to fiber-switching technology. As a consequence, we decided to exclude from our analysis those methods whose working principle needs the use of any kind of mechanical movement.

Our initial formulation of optical performance specifications that are applicable to such a TTFF can be derived by taking into account the routing needs of a dense WDM fiber-optic network. Our preliminary analysis led to the following items:

A tuning range between 0.4 nm (commutation between two 50-GHz adjacent channels) and 2.8 nm (fully operational eight-channel OXC).

A response time of less than 10 ms.

The authors are with the Institut Fresnel, Unité Mixte de Recherche 6133, Centre National de la Recherche Scientifique, Ecole Nationale Supérieure de Physique de Marseille, Domaine Universitaire de Saint Jérôme, 13397 Marseille Cedex 20, France. M. Lequime's e-mail address is michel.lequime@fresnel.fr.

Received 1 October 2001.

0003-6935/02/163277-08\$15.00/0

© 2002 Optical Society of America

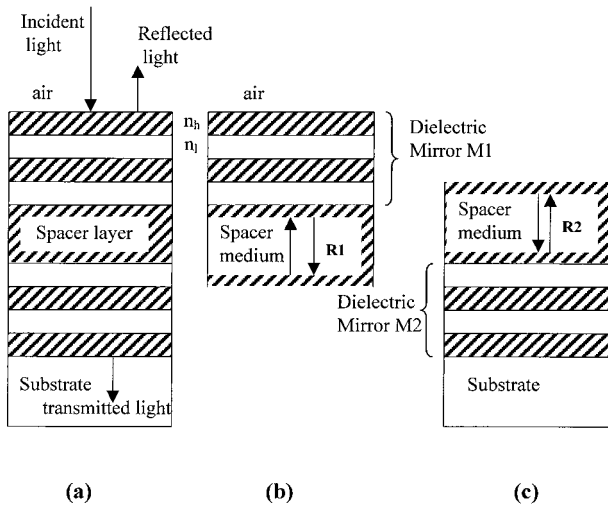


Fig. 1. Design of a single-cavity filter: (a) Fabry Perot single-cavity filter, (b) structure 1 with the first dielectric mirror, (c) structure 2 with the second dielectric mirror. Note that the the spacer is the incident medium for structures 1 and 2.

Optical performances in accordance with typical DWDM narrow-band filter requirements, i.e., ≤ 1.0 -dB insertion loss and ≥ 0.25 -nm at relative bandwidth at -0.5 dB and ≤ 0.6 -nm relative bandwidth at -25 dB.

2. Concept Analysis

A. Theoretical Approach

A thin-film bandpass filter includes one or more Fabry–Perot resonant cavities, each of which consists of a spacer layer surrounded by two reflectors. The optical thickness of the spacer is closely connected to the central wavelength λ_c of the filter (as a first approximation, it is a multiple of the half-wavelength). Moreover, each reflector is made of a stack of dielectric layers, each having an optical thickness equal to a quarter-wavelength with a refractive index that corresponds alternatively to a high (H) and low (L) level. The spacer is generally made of one of the dielectric materials used in reflector stacks. As a consequence, it is possible to describe a single-cavity narrow-bandpass filter (NBPF) by the following synthetic formula:

$$(HL)^q - 2pH - (LH)^q \quad (1)$$

One can tune such a filter by changing the optical thickness of the spacer ($2pH$), but it is possible that the external action used to achieve this change can also induce some modifications to the optical properties of the mirrors layers (for example an identical increase in the refractive index of all the H layers and a slight decrease in the refractive index of all the L layers).

A complete analysis of such phenomena is thus needed to understand and predict the exact relation between the relative optical thickness change and the

relative modification of the central wavelength of the TTFF.

Let us consider the single-cavity filter design in Fig. 1. All the media are supposed to be dielectric and absorption free. The refractive index of the incident medium is $n_0 = 1$ (air), the refractive index of the substrate is n_s , and the structure is the association of several alternate dielectric layers of refractive index n_h and n_l . We suppose that the multilayer is illuminated under normal incidence at a λ wavelength.

We can separate the structure of the multilayer into three parts: a set of quarter-wavelength layers (mirror 1), a spacer, and a second set of quarter-wavelength layers (mirror 2). This dissociated analysis, called the partitioning method,² permits one to consider the multilayer as a Fabry–Perot cavity filter and to use known results of the Fabry–Perot interferometer.³

Transmission T of the whole structure depends on the characteristics of mirrors M1 between the spacer medium and the air [see Fig. 1(b)], M2 between the spacer medium and the substrate [see Fig. 1(c)], the optical thickness of the spacer layer $n_h t_{sp}$, and the incident wavelength:

$$T = \frac{T_{\max}}{1 + F \sin^2 \phi}, \quad (2)$$

where

$$F = \frac{4\sqrt{R_1 R_2}}{(1 - \sqrt{R_1 R_2})^2}, \quad T_{\max} = \frac{T_1 T_2}{(1 - \sqrt{R_1 R_2})^2},$$

$$\phi = \frac{2\pi}{\lambda} n_h t_{sp} + \frac{\delta_1 + \delta_2}{2}, \quad (3)$$

R_1 is the reflectance of structure 1 (spacer medium/M1/air) [Fig. 1(b)], R_2 is the reflectance of structure 2 (spacer medium/M2/substrate) [Fig. 1(c)], T_1 and T_2 are the transmittance of structures 1 and 2, and δ_i ($i = 1, 2$) is the phase of the complex reflection amplitude coefficient r_i defined for the electric field of structure i :

$$r_i = \sqrt{R_i} \exp j\delta_i. \quad (4)$$

Note that R_i and δ_i have real values. From Eq. (2) one can deduce that the maximum transmittance of the whole structure occurs when $\phi = p\pi$, $p = 0, \pm 1, \pm 2, \dots$. So the wavelengths of maximum transmittance satisfy

$$\lambda = \frac{2n_h t_{sp0}}{p - \frac{\delta_1 + \delta_2}{2\pi}}, \quad (5)$$

where p is an integer.

At wavelength λ_0 , the design of the structure leads to $\delta_i = 0[\pi]$ rad. Since the spacer was designed as a

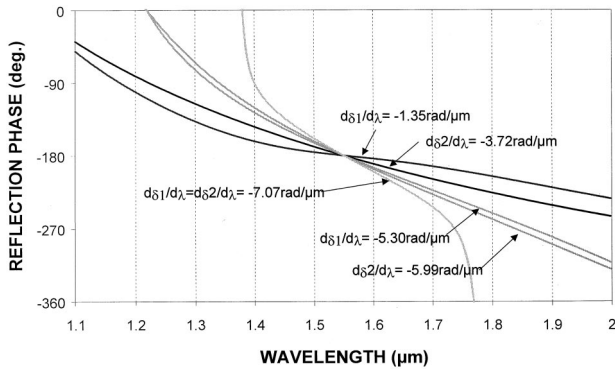


Fig. 2. Variation of the phase reflection coefficients with respect to the wavelength for various q values. Phase reflection coefficients δ_1 and δ_2 for $(HL)^q$ mirrors (structures 1 and 2 are defined in Fig. 1): boldface curve, $q = 2$; black curve, $q = 4$; lightface curves, $q = 16$. The refractive indices are $n_h = 2.1$ and $n_l = 1.5$. The incident medium is the high-index medium $n_0 = 2.1$. The index of the substrate medium is $n_s = 1$ for structures 1 and $n_s = 1.45$ for structures 2. The central wavelength is $\lambda_0 = 1.55 \mu\text{m}$. The phase dispersion at $\lambda = \lambda_0$ increases with the number of layers.

half-wavelength, Eq. (5) is satisfied. Hence, for such a structure,

$$\lambda_0 = \frac{2n_h t_{sp0}}{p} \quad (6)$$

is a wavelength of maximum transmittance.

By using Eq. (5) one can approximately evaluate the shift of the maximum transmittance wavelength $\Delta\lambda$ as a function of the small optical thickness modification of spacer $\Delta(nt_{sp})$:

$$\frac{\Delta\lambda}{\lambda_0} = \kappa \frac{\Delta(nt_{sp})}{nt_{sp0}}, \quad (7)$$

where

$$\kappa = \frac{1}{1 - \frac{\lambda_0}{2\pi p} \frac{\partial(\delta_1 + \delta_2)}{\partial\lambda}}. \quad (8)$$

So variation of the maximum transmittance wavelength depends, to a first approximation, not only on the spacer thickness modification, but also on the dispersion phase of the mirrors above and below the spacer layer. With the values of conventional dielectric index materials, the phase derivative of the mirrors exhibits negative values, and the relative spectral shift is always smaller than the relative thickness variation ($\kappa \leq 1$). A thicker spacer and mirrors with small phase dispersion around the central wavelength are two ways to increase the spectral shift up to 1. We now illustrate this spectral shift by use of various numerical examples.

The first example describes the behavior of a single-cavity structure $[(HL)^q - 2pH - (LH)^q]$ when quantities p or q are changed. The refractive indices are $n_h = 2.1$, $n_l = 1.5$, and $n_s = 1.45$ and the central wavelength $\lambda_0 = 1.55 \mu\text{m}$. In Fig. 2 we have plotted

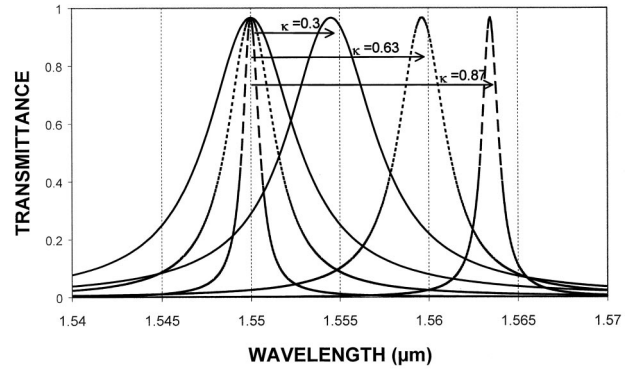


Fig. 3. Variation of the spectral shift of a filter with respect to the thickness of the spacer layer. Transmittance versus wavelengths for several spacer thicknesses $(H B)^6/2pH/(H B)^6$ when t_{sp} increases by 1%: solid curves, $p = 1$; short dashed curves $p = 4$; long dashed curves, $p = 16$. The central wavelength is $\lambda_0 = 1.55 \mu\text{m}$. The relative spectral shift increases with number p .

the phase reflection coefficients δ_1 and δ_2 for the two mirrors for several values of q . If we increase the numbers of layers of each mirror from $q = 2$ to 16, the phase dispersion also increases but only moderately. Now if one maintains a constant mirror geometry (for example, to $q = 6$), the spectral shift of the maximum transmittance of the Fabry–Perot cavity is widely dependent on the thickness of the spacer layer (see Fig. 3). The maximal relative spectral shift obtained for high values of p is equal to the relative thickness variation of the spacer ($\kappa = 1$).

The second example is a study of the relative spectral shift for a given cavity design $[(HL)^6 - 8H - (LH)^6]$ corresponding to $p = 4$ and $q = 6$. Four possibilities are considered: the first already analyzed above is when only the thickness of the spacer layer is changed. The relative spectral shift is equal to 62% of the relative thickness variation (filled circles

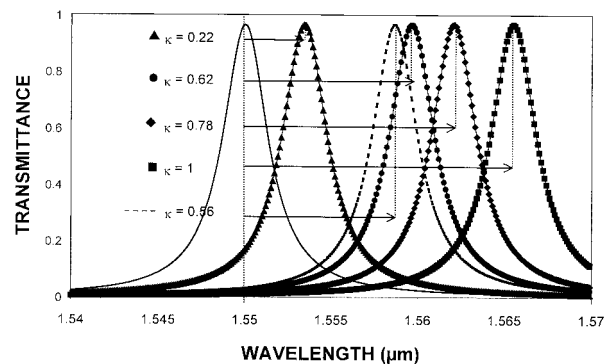


Fig. 4. Transmittance versus wavelength for a $(HL)^6 - 8H - (LH)^6$ Fabry–Perot cavity when the thickness of several layers is changed: boldface curve, starting design centered at $\lambda_0 = 1.55 \mu\text{m}$; triangles, the thickness of the 12 low-index layers increased by 1%; circles, only the thickness of the spacer layer (8H) increased by 1%; diamond, the thickness of the 13 high-index layers increased by 1%; squares, all the thicknesses increased by 1%; the cavity is centered at $\lambda_0 + 1\%$; dashed curves, the thickness of the 13 high-index layers increased by 1%, whereas the thickness of the 12 low-index layers decreased by 1%.

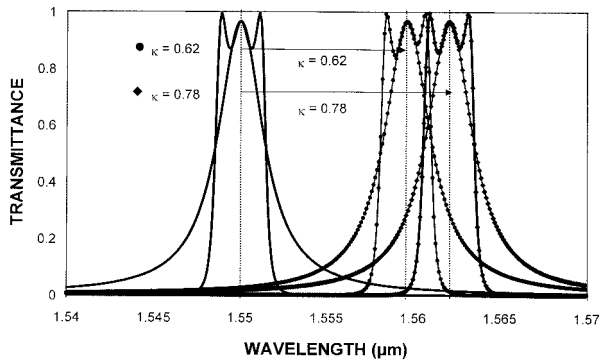


Fig. 5. Transmittance versus wavelength for a $(HL)^6 - 8H - (LH)^6$ Fabry-Perot single and triple cavity when the thickness of several layers changes: solid curve, starting design centered at $\lambda_0 = 1.55 \mu m$; circles, only the thickness of the spacer layer (8H) increased by 1%; diamonds, the thickness of the 13 high-index layers increased by 1%.

in Fig. 4). When we changed all the high-index layer thicknesses, the relative spectral shift improved to 78% of the relative thickness variation (filled diamonds in Fig. 4). This is an intermediate value between the first case and the case in which all the thicknesses are changed ($\kappa = 1$; filled squares in Fig. 4). Finally if only low refractive-index layers show variable thicknesses the κ factor does not exceed 22% (filled triangles in Fig. 4). This case is obviously the less favorable for optical tuning applications. Finally, we studied a hypothetical case in which the opposite effect between high- and low-index layers is expected. In this case the relative spectral shift is equal to 56% of the relative thickness variation of each layer.

This analysis is also applicable for multiple-cavity filters. Figure 5 shows the spectral response of the previous structure $[(HL)^6 - 8H - (LH)^6]$, but in a single-cavity and a triple-cavity arrangement. Two cases are represented: when the three relative spacer thicknesses increase by 1% (circles) and when all the high-index layer thicknesses increase by 1% (diamonds). In both cases, the value of κ is the same for a single-cavity or a triple-cavity structure. However, one can note that the spectral response of the triple cavities is slightly damaged because of the possible high relative thickness variation (1%).

In conclusion, by changing the spacer thickness of a Fabry-Perot cavity filter, one can modify its central wavelength. The spectral shift depends on the geometry of the structure. For tunable applications, the relatively small thickness variation (approximately 0.1% at most) requires structures with a maximal spectral shift. The best configurations are those with either thick spacers or only a few mirror layers. The solution that must be chosen for dense WDM applications is of course the first one.

B. Driving Parameters

Many physical parameters can be used to achieve the optical thickness changes required to spectrally tune a thin-film filter. We chose to focus our trade-off

analysis on the two most attractive, i.e., the temperature and the electric field.

The modification of temperature applied to a thin-film filter induces various changes in the optical properties of all its layers. We can distinguish between the direct effects, such as the expansion of the layer thickness and the refractive-index change, and the indirect effects associated with the thermal properties of the substrate. The thermal expansion of the substrate induces a decrease in the thickness of these same layers and to a lesser degree a change in their refractive index that is due to strain-optic phenomena). Takashashi⁴ developed a simplified model that allows for the determination of which kind of substrate should be used for a standard bandpass filter to cancel the thermal drift of the central wavelength. By using the same model, we can try to maximize these thermal effects by an appropriate choice of substrate as well as material for the multilayer stack and achieve this by means of a large tuning range (see Section 3).

Use of an electric field as a driving signal must have the optical properties of one or more layers be sensitive to such a parameter. This can be achieved as follows (see Section 4):

Either by use of the piezoelectric effect, and in this case we again distinguish between the direct effect (change in physical thickness of a piezoelectric spacer, for example) and the indirect effect (change in thickness of all the layers, induced by a modification of the transverse dimensions of a piezoelectric substrate).

Or by use of the electro-optic effect with which the electric field provides for example, a change in refractive index of all the high-index layers, spacer included.

3. Temperature Effects

As indicated above, the thermal shift of NBPFs has been previously studied by Takashashi with the help of a simplified model, which enables calculation of the temperature stability of the center wavelength (TSCW) as a function of the coefficient of linear expansion (CLE) of the substrate, the coefficient of linear expansion of the film, the temperature coefficient of the refractive index, and the Poisson ratio of the film.

In Takashashi's model, all the layers of a NBPF are considered as a single layer deposited on a substrate. Properties of this single layer are calculated from each real layer's properties according to Macleod's calculation for refractive-index values in Fabry-Perot cavity filters,⁵ and mechanical values are weighted mean-layer values. Then calculation of the thermal sensitivity of this single layer takes into account the mechanical expansion of the layers, the mechanical expansion of the substrate as well as its result on equivalent single-layer thickness through elastic strain relations and finally the refractive-index modification induced by the temperature.

By using the Takashashi model, we were able to compute the variations of the TSCW factor of a

Table 1. Filter Sensitivities

Sensitivity	Filters		
	F_0	F_1	F_2
Thermal (pm/°C)	17	51	37
Strain (pm/μ ϵ)	-1.2	-2.2	-1.7

single-cavity NBPF (Ta₂O₅-SiO₂) with respect to the CLE of the substrate. If the design of this TFF (called F_0) is described by the stack formula [(HL)⁸ - 10H - (LH)⁸], corresponding to a full width at half-maximum (FWHM) of approximately 0.4 nm, the TSCW factor of such a filter varies between 17 pm/°C for an ideal substrate with zero CLE and 0 pm/°C for substrates dedicated to the WDM applications (such as Schott S7003 or S7006)⁶ and characterized by a CLE of around 10⁻⁵/°C. The first value determines the intrinsic thermal sensitivity of the NBPF (in our case, 17 pm/°C), the second allows for the evaluation of its strain sensitivity (here -1.7 pm/μ ϵ , i.e., -17 pm/°C divided by 10 × 10⁻⁶/°C).

To achieve thermally tunable components, we tried to maximize both effects by selecting film materials with a high intrinsic thermal sensitivity and a good strain sensitivity as well as a special substrate having a high and negative CLE.

We now consider the use of silicon (Si)⁷ as high-index material in a multilayer stack (retaining SiO₂ as the low-index material). At 1.55 μm, the refractive index of Si is 3.52 and the normalized thermal coefficient of refractive index equals 3.9 × 10⁻⁵/°C (because of the lack of data for thin films, we used crystal figures). This value is greater than seven times higher than for Ta₂O₅. The silicon CLE is 2.6 × 10⁻⁶/°C, greater than five times the value used for Ta₂O₅ thin film. We also used the silicon crystal value for the Poisson ratio, i.e., 0.28. By using all these data, we calculated the intrinsic thermal and strain sensitivities for two new filter designs having the same spacer optical thickness and almost the same FWHM (around 0.4 nm), but one (F_1) has a high-index Si spacer [(HL)³ - 10H - (LH)³], whereas the other (F_2) has a low-index SiO₂ spacer [(HL)³H - 10L - H(LH)³]. The results of these computations are summarized in Table 1. To maximize the effects of the substrate, we propose to use a glass ceramic material with a negative thermal expansion coefficient, such as the NEX-C from Ohara Corporation⁸ (with a CLE of approximately -20 × 10⁻⁷/°C). This material presents a high internal transmittance (99.3% at 1570 nm for a 10-mm thickness) and can be used as a substrate for the previous Si-SiO₂ thin-film filter.

By combining both effects, we were also able to develop a thermally TFF with a sensibility of approximately 55 pm/°C. Temperature excursions as low as 50 °C would also be sufficient to fulfill the tentative specifications proposed in Section 1.

In practice, the temperature modification of a given filter can be achieved by the combination of local heating (through thin resistive electrodes such as

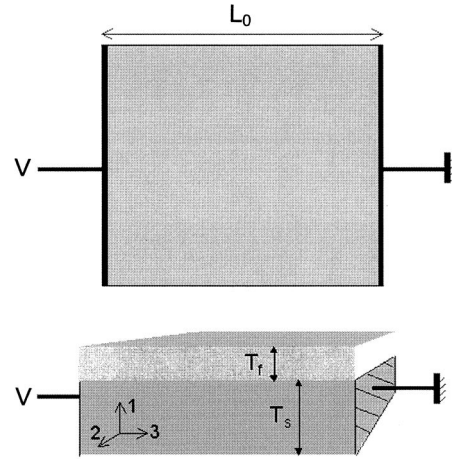


Fig. 6. Schematic view of a NBPF deposited on a piezoelectric substrate: T_s , substrate thickness and T_f , stack thickness.

those used in silica-based thermo-optic switches) and a global regulation mean (such as a Peltier cooler) providing, for example, a relatively low temperature and used to accelerate the cancellation of the effect of a previous heating phase. Obviously, great care must be taken with the thermal isolation, temperature control, and regulation to lock the TFF on a given wavelength. Moreover, if we use a combination of transparent electrodes and a stable substrate, it seems possible to achieve a response time as short as 10 ms in the heating phase because the active layers are not thick. For the cooling phase a longer response time is expected because the substrate makes a greater contribution. Obviously, all these items have to be assessed experimentally.

4. Electric Field Effects

A. Piezoelectric Effect on the Substrate

A possible way to tune the central wavelength of a thin-film NBPF can be derived from the previous interpretation of Takashashi's modeling of the NBPF's temperature stability. In fact, the role played by temperature expansion of the substrate can be replaced by piezoelectric substrate dimension change. In this case, the physical expansion of the substrate is no longer isotropic but depends on the structure of the piezoelectric tensor. By simply adapting the previous elastic strain model to this new constraint, we were able to predict the relation between the induced center wavelength shift and the amplitude of the applied electric field to such an active substrate.

We studied a thin-film filter deposited on a piezoelectric substrate as described in Fig. 6. For the sake of simplicity, we describe the substrate piezoelectricity by the two-coefficient tensor \mathbf{d} , defined as

$$\frac{\Delta L_3}{L_0} = d_{33}\epsilon_3, \quad (9)$$

$$\frac{\Delta L_2}{L_0} = d_{32}\epsilon_3, \quad (10)$$

where ΔL_i is the length variation along the i axis and the applied electric field ϵ_3 equals V/L_0 .

As did Takashashi, we define the NBPF equivalent single layer with its Poisson ratio ν and its Young's modulus E . When external voltage V is applied, it results in a dimension change of the substrates that involves a stress \mathbf{t} within the film (the \mathbf{t} tensor is supposed to have two components, t_2 and t_3). We express the center wavelength shift as

$$\frac{\Delta\lambda_\epsilon}{\lambda_0} = \frac{\Delta(n_\epsilon T_f^\epsilon)}{n_0 T_f^0}, \quad (11)$$

where subscript or superscript ϵ refers to quantities when an electric field is applied.

So we need to calculate the average refractive index of the single layer that describes the NBPF and its thickness variation before and during application of electric field. Following the same process developed by Takashashi,⁴ we define the average refractive index of the NBPF n , the average packing density $P = V/L_0^2 T_f$, where V is the volume actually occupied by evaporated material, and the average refractive index of that portion of the NBPF that is actually occupied by film material N (see Ref. 5). Equation (12) gives the relation between n and N :

$$n = NP + 1 - P. \quad (12)$$

To evaluate the center wavelength shift, we must express average refractive index n_ϵ and the modified NBPF thickness T_f^ϵ as functions of electric field ϵ . Thus we also need to calculate a new average packing density P_ϵ .

Elasticity equations lead to

$$L_1 = T_f \left[1 - \frac{\nu(t_2 + t_3)}{E} \right], \quad (13)$$

$$L_2 = L_0 \left(1 + \frac{t_2 - \nu t_3}{E} \right), \quad (14)$$

$$L_3 = L_0 \left(1 + \frac{t_3 - \nu t_2}{E} \right). \quad (15)$$

From Eqs. (9), (10), (14), and (15) we deduce that

$$t_2 = E \frac{d_{32} + \nu d_{33}}{1 - \nu^2} \epsilon, \quad (16)$$

$$t_3 = E \frac{d_{33} + \nu d_{32}}{1 - \nu^2} \epsilon, \quad (17)$$

so that elasticity equations can be rewritten as

$$L_1 = T_f \left[1 - \frac{\nu}{1 - \nu} (d_{32} + d_{33}) \epsilon \right], \quad (18)$$

$$L_2 = L_0 [1 + d_{32} \epsilon], \quad (19)$$

$$L_3 = L_0 [1 + d_{33} \epsilon]. \quad (20)$$

When the electric field is applied, the resultant stress causes a change in film volume which becomes V_ϵ . This modified volume expression can be calculated from Eqs. (18)–(20), and, if we simplify and keep only first-order terms, it becomes

$$V_\epsilon = V_0 \left[1 + \frac{1 - 2\nu}{1 - \nu} (d_{32} + d_{33}) \epsilon \right]. \quad (21)$$

The average packing density of the film already defined by the ratio of volume occupied by real material V divided by geometric volume $V_0 = L_0^2 T_f$ when no electric field is applied or by V_ϵ in the case of electrical excitation can then be calculated from Eq. (21):

$$P_\epsilon = \frac{V}{V_\epsilon} = P_0 \left[\frac{1}{1 + \frac{1 - 2\nu}{1 - \nu} (d_{32} + d_{33}) \epsilon} \right]. \quad (22)$$

The average refractive index of the NBPF when the electric field is applied, defined by $n_\epsilon = N_0 P_\epsilon + 1 - P_\epsilon$, becomes

$$n_\epsilon = 1 + \left[\frac{P_0}{1 + \frac{1 - 2\nu}{1 - \nu} (d_{32} + d_{33}) \epsilon} \right] (N_0 - 1). \quad (23)$$

Finally, we have to consider only film thickness change given by Eq. (13) and the average refractive-index modification given by Eq. (23) to calculate the center wavelength shift of Eq. (11). Assuming that $P_0 = 1$, we obtain

$$\Delta\lambda_\epsilon = \lambda_0 \left(\frac{1}{N_0} \left\{ 1 + \frac{N_0 - 1}{1 + \frac{1 - 2\nu}{1 - \nu} (d_{32} + d_{33}) \epsilon} \right\} \times \left[1 - \frac{\nu}{1 - \nu} (d_{32} + d_{33}) \epsilon \right] - 1 \right). \quad (24)$$

This relation allows us to compute the relative spectral shift of the filter with respect to the amplitude of the electric field applied along the three axes (lateral dimension of the substrate). We note that the right parameter in this case is the effective piezoelectric coefficient, i.e., the sum of both piezoelectric coefficients that describe the in-plane deformations of the substrate.

Several materials present piezoelectric activity (such as quartz, barium titanate, lithium niobate, zinc oxide), but we must obviously select a material that is transparent in the telecommunications band (almost the C band) and whose effective piezoelectric coefficient is as high as possible. With respect to both criteria, lithium niobate and barium titanate are the most promising candidates.

The tuning range of such a filter is limited by the maximum voltage that can be applied to the piezo-

electric substrate without degradation. Commercial piezoelectric ceramics admit a voltage limitation beyond which ceramics can be depolarized (depoling effect). A typical operating limit is between 1 and 20 kV/mm. With such a value, a strain of the order of 0.2% can be achieved. The voltage limitation for piezoelectric layers coated on substrates by different techniques is due to the electric breakdown of the coating: a typical value of 10 kV/mm is generally assumed. To keep some safety margin, we propose to maintain the maximum strain value below 1000 $\mu\epsilon$ (i.e., 0.1%) and the electrical field below the breakdown voltage.

We propose to reuse the F_0 NBPF as described in section 3, that is, $[(HL)^8 - 10H - (LH)^8]$, where H represents a Ta_2O_5 quarter-wavelength layer and L represents a SiO_2 quarter-wavelength layer. In addition let us suppose that the effective piezoelectric coefficient of the active substrate is approximately 200 pm/V and that for this active substrate we adopt the usual dimensions for a WDM filter (1.4 mm \times 1.4 mm \times 0.8 mm). In such a case, we can reach a tuning range of approximately 0.4 nm with a maximum driving voltage of 3.5 kV (corresponding to an electric field of 2.5 kV/mm). Taking into account the standard bandwidth of classical piezoelectric structures, the response time of such a TTFF would also be in accordance with the specifications outlined in Section 1.

Despite this relatively narrow tuning range and the need for high driving voltages, this solution is quite attractive, because it uses classical NPBF structures (except for the substrate), well-known manufacturing procedures, standard metallic electrodes (no high transmittance requirement, taking into account their lateral disposition), and it is also well matched to the requirements of an active add/drop multiplexer.

B. Piezoelectric Effect on the Spacer

Another possibility to exploit the dimensional change associated with the piezoelectric effect is to use a piezoelectric material as the spacer inside a thin-film filter. Provided that the thickness of this spacer and the number of reflectors is in accordance with the recommendations outlined in Section 2, a low driving voltage (typically 10 V) should be sufficient to generate a relatively large center wavelength shift.

The main problem of such a solution is to overcome the cancellation of the piezoelectric effect at the macroscopic scale that is due to the deposition process that can lead to either an amorphous substance without intrinsic piezoelectric activity or a polycrystalline layer with crystallite random orientation. A dedicated electron-beam deposition procedure has allowed us to obtain tantalum pentoxide layers with noticeable piezoelectric activity (typically 13 pm/V).⁹ Such a feature allows us to achieve a spectral shift of 0.1 nm if we restrict the applied electric field to less than half of the breakdown limit (i.e., 5 kV/mm). Improvement of our deposition process should allow

us to reach bigger values that would be close to the nanometer range.

A key question raised by the use of such active spacers concerns the design of the electrodes. To reach low driving voltages, the electrodes must be as close as possible to these active layers. They must be crossed by the light beam and should have good transmittance properties in the C band. The use of indium tin oxide (ITO) electrodes on both sides of the multilayer stack provide us with a realistic solution, if we take into consideration its optical properties and its compatibility with a deposition process. Moreover, the use of only two electrodes allows us to apply the same electric field to the different spacers of a multiple-cavity NBPF.

C. Electro-Optic Effect on the Spacer

In a 1999 theoretical paper, Sakaguchi and Kubo proposed a NBPF active configuration¹⁰ using thin barium titanate crystal ($BaTiO_3$) as high-index layers (spacer included) and silicon dioxide (SiO_2) or magnesium oxide (MgO) as low-index layers. They assumed that the c axis of the $BaTiO_3$ crystal is parallel to the z axis (i.e., perpendicular to the layer's plane) and that the electric field is applied along the x axis. Such orientation allows one to take advantage of the extremely large electro-optic coefficient r_{51} of this material (between 1300 and 1640 pm/V) and to avoid the use of transparent electrodes. Approximately 6-nm tuning ranges could be reached for an applied field of 4 kV/mm.

Such a solution is attractive in terms of tuning range and response time (because of the high bandwidth of the electro-optic effect), but its practical implementation raises some serious problems, such as the polarization dependence of all the filter properties (especially the central wavelength of the filter and the losses) and the manufacture of the active high-index layers through a standard vacuum deposition process. Another possible solution consists in the use of nanoscopic polymer-dispersed liquid crystals as a spacer layer.¹¹

5. Conclusion

Efficient tunable narrow-bandpass thin-film filters can be developed by use of combined thermal effects on both the layers and the substrate (highly sensitive Si/SiO₂ layers deposited on a glass ceramic substrate with a negative CLE), strain sensitivity of standard alternate Ta₂O₅/SiO₂ layers activated by dimensional changes in a piezoelectric substrate (lithium niobate or barium titanate), or a change in the piezoelectric thickness of a cavity spacer driven by an electric field applied through transparent ITO electrodes. Tuning in the nanometer range seems realistic for the various configurations. Experimental assessments of all these capabilities are now in progress⁹ in our laboratory.

References and Notes

1. See, for example, DiCon Fiberoptics, Inc. communication products page on motorized tunable bandpass filters at <http://www>.

- diconfiberoptics.com/products/index_measurement.htm.
2. P. Baumeister, *Optical Coating Technology*, UCLA short Course, Library of Congress Catalog No. TS 517.2 B38 2000 (Library of Congress, Washington, D.C., 2001), Chap. 2.
 3. M. Born and E. Wolf, *Principles of Optics*, 6th ed. (Pergamon, New York, 1993), Chap. 7.
 4. H. Takashashi, "Temperature stability of thin-film narrow-bandpass filters produced by ion-assisted deposition," *Appl. Opt.* **34**, 667–675 (1995).
 5. H. A. Macleod, *Thin-Film Optical Filters*, 2nd ed. (Macmillan, New York, 1986), Chap. 9, pp. 405–406.
 6. See the Schott telecom materials S7003 datasheet at <http://us.schott.com/sgt/english/products/s7003.html>.
 7. See Ioffe Physico-Technical Institute, physical properties of semiconductors, silicon properties at <http://www.ioffe.rssi.ru/SVA/NSM/Semicond/Si/>.
 8. See the Ohara Corporation Homepage link to the Nex-C product page at http://www.ohara-inc.co.jp/ohara_e/ohara.htm.
 9. R. Parmentier, F. Lemarchand, M. Cathelinaud, M. Lequime, C. Amra, S. Labat, S. Bozzo, F. Bocquet, A. Charai, O. Thomas, and C. Dominici, "Study of piezoelectric tantalum pentoxide thin films for optical tunable applications," *Appl. Opt.* **41**, 0000–0000 (2002). OT 17995, same issue.
 10. S. Sakaguchi and S. Kubo, "Transmission characteristics of multilayer films composed of electro-optic and dielectric materials," *Opt. Commun.* **170**, 187–191 (1999).
 11. K. Lewis, G. Smith, and I. Mason, "Progress in the realization of frequency agile filters using nanoscopic polymer dispersed liquid crystals," in *Optical Interference Coatings*, Postconference Digest, Vol. 63 of OSA Trends in Optics and Photonics Series (Optical Society of America, Washington, D.C., 2001).